COMPDYN 2025
10th ECCOMAS Thematic Conference on
Computational Methods in Structural Dynamics and Earthquake Engineering
M. Papadrakakis, M. Fragiadakis (eds.)
Rhodes Island, Greece, 15-–18 June 2025

DYNAMIC ELECTROACTIVE METAMATERIALS WITH FLEXOELECTRIC AND PIEZOELECTRIC MICROSTRUCTURES

E. Rohan[1], **A. Hosseinkhani**[1], **and R. Cimrman**[2]

[1]Department of Mechanics, NTIS New Technologies for Information Society, Faculty of Applied Sciences, University of West Bohemia, Univerzitní 8, 306 00 Pilsen, Czech Republic
e-mail: rohan@kme.zcu.cz

[2]Institute of Thermomechanics, Czech Academy of Sciences, Dolejškova 1402/5, 18200, Prague 8, Czech Republic
e-mail: cimrman3@ntc.zcu.cz

Keywords: Flexoelectric, Piezoelectric, Homogenization, Band gaps, Metamaterial

Abstract. *We consider periodic microstructures composed of flexoelectric, or piezoelectric materials and involving electrodes which enable for control of the response due to the electromechanical transmission and tunable external electric circuits. The asymptotic homogenization is employed to derive models describing the effective properties of such metamaterials. Piezoelectric or dielectric materials with a weak flexoelectric property, constituting the skeleton of general periodic porous structures enable to generate the strain gradients. Using the asymptotic homogenization, it is shown that effective behaviour of such materials is piezoelectric, whereby the homogenized piezoelectric coefficients are computed using the characteristic responses of the flexoelectric microstructure.*

1 INTRODUCTION

Conventional materials propagate waves with very limited attenuation and are not able to effectively damp or manipulate wave propagation. Metamaterials are characterized by periodic microstructures which, although composed of conventional materials, due to appropriate microstructural design, provide astonishing macroscopic features such as negative refraction, negative equivalent moduli, and negative equivalent density; this last property give rise to the "anti-resonance" effect and, consequently, to the frequency band gaps [1]. However, these features do not contain the flexibility to change or tune the wave propagation according to the loading frequencies. An extension of passive metamaterials to electroactive metamaterials provides several options to both tune and change their dynamic response in real-time applications [2, 3].

Combination of passive elastic metamaterials with electroactive materials enriches the wave control abilities of heterogeneous structures and paves the way for designing waveguides, directional vibration insulators, and one-way filters. In this regard, an external electric circuit, also known as a shunting circuit connected to such structures and involving tunable resistors, inductors, and capacitors, can modify the effective mechanical properties of the whole structure and, thus, provides an opportunity for adjusting band gaps [2, 4]. Moreover, the electrical field can be applied through boundary conditions to tune the band gap properties instead of changing the material or geometry of a heterogeneous structure. The employment of *phononic crystals* (PCs) along with piezoelectricity can be designed with a multi-objective criterion, to work efficiently in several simultaneous applications, such as simultaneous vibration control and energy harvesting [3, 5].

Besides the piezoelectric materials, the flexoelectric microstructures can be considered to provide the electromechanical coupling. The flexoelectricity is a property of all dielectric materials, occurring in both centrosymmetric and asymmetric crystals when strain gradient is generated. Conversely, also a "hyperstress" is generated due to gradient of electric field, contributing to the material stiffness. Both these direct and reverse effects appear at small scales, rather then at the "macro-level". Physics of the flexoelectric materials has been studied recently within the thermodynamic framework in [6], where the complexity of the interface and boundary conditions has been explored for various types of the flexoelectric constitutive laws.

The aim of this short paper is two-fold. Firstly we show an example of electroactive metamaterial plate based on the "resonance effect" due to the high contrast in the elasticity and on the piezoelectric sensor/actuator components which can be interconnected using an *external electric circuit* (EEC). We illustrate, how the frequency bang gaps in the wave propagation can be modified by an EEC. The electromechanical coupling, namely the transformation of local strains into local electric field can be ensured by flexoelectric microstructures. We show that a suitable microstructure give rise to an "effective" piezoelectric behaviour. The asymptotic homogenization method [7] is employed to explore behaviour of weakly flexoelectric periodically heterogeneous materials, *cf.* [8, 9] analogous treatment of "controllable weakly piezoelectric metamaterials" . Related works appeared recently, see *e.g.* [10, 11, 12], including higher order homogenization which naturally leads to effective constitutive laws involving higher-order gradients. Therefore, the effective flexoelectric mathematical models can be obtained by upscaling heterogeneous piezoelectric materials, [13]. However, it has been demonstrated in [14] using numerical simulations, that piezoelectric metamaterials can be designed by lattice periodic structures made of dielectric materials exhibiting the flexoelectricity. The present study reported here confirms this qualitative result by the homogenization. Analytic result is derived

for a 1D periodic rods designing a porous structure.

2 ELECTROACTIVE PIEZOELECTRIC METASTRUCTURES FOR BAND GAP CONTROL

As illustrated in Fig 1, a two-dimensional heterogeneous plate consisting of a piezoelectric matrix and non-piezoelectric inclusions is considered [5]. The band gap diagram is evaluated

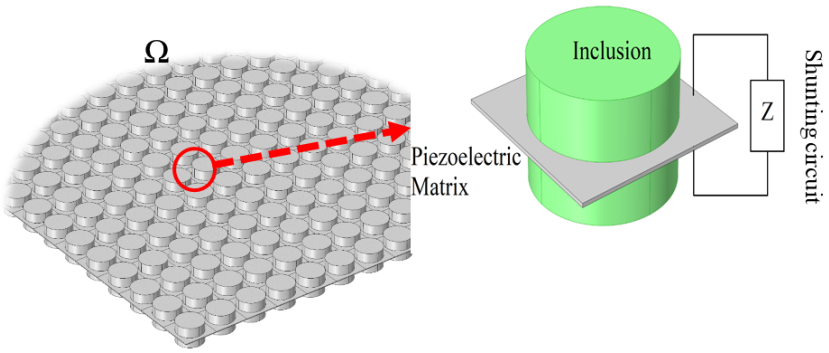

Figure 1: Periodic structure of the electroactive composite and one reference cell.

for this configuration and presented in Fig 2. To investigate the impact of the piezoelectric feature on band gap characteristics, we compare the band gap (BG) diagrams of the unit cell with pure-elastic matrix and the one with piezoelastic matrix.

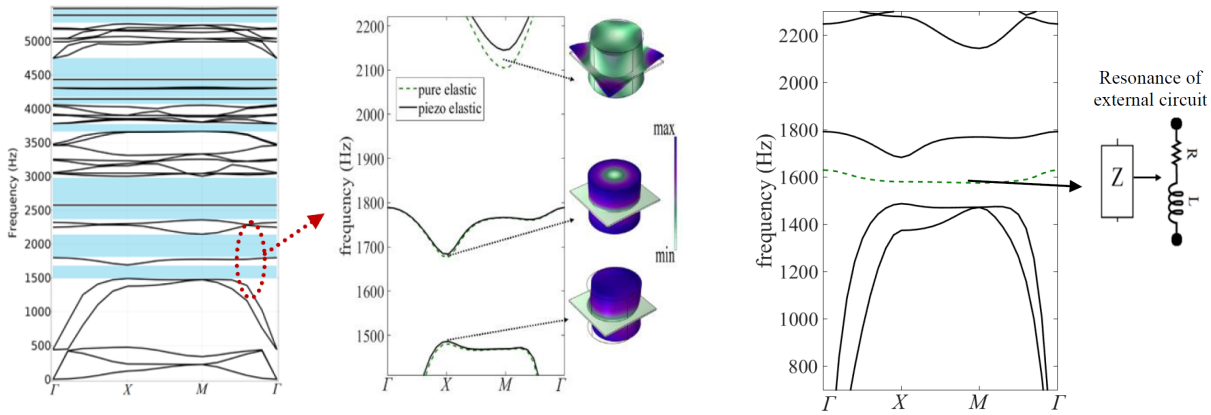

(a) (b)

Figure 2: (a) Band gap diagram and comparison between pure elastic and piezoelectric elastic cases (b) Appearance of a resonance curve due to the external circuit.

The BG diagram for the pure-elastic case can be obtained by setting the piezoelectric coupling tensor to zero. Fig 2 a illustrates the effect of the coupling tensor on band gap properties, with a focus on the first two band gaps. A moderate difference of 40 [Hz] is observed between the third mode of the pure-elastic (2105 [Hz]) and piezoelastic (2145 [Hz]) cases. Another interesting feature enabled by the external circuit is the introduction of a new resonance branch in the band gap diagram. A simple circuit containing a resistor and an inductor in series can

create this branch as shown in Fig 2 b. In the example with $R = 10[kOhm]$ and $L = 1.3[H]$, the branch frequency is set to around 1600 [Hz].

2.1 Self-powered meta-structure

In this section, we investigate how the vibrations can be attenuated using the piezoelectric meta-plate property which enables to connect responses at two (or more) distant point by electric circuits (Fig 3). The coupling is made by an electric circuit (EC) represented by an impedance associated with the standard elements: capacitors, inductors, and resistors arranged in series and parallel branches. The electroactive metastructure is influenced by the electrodes connecting the

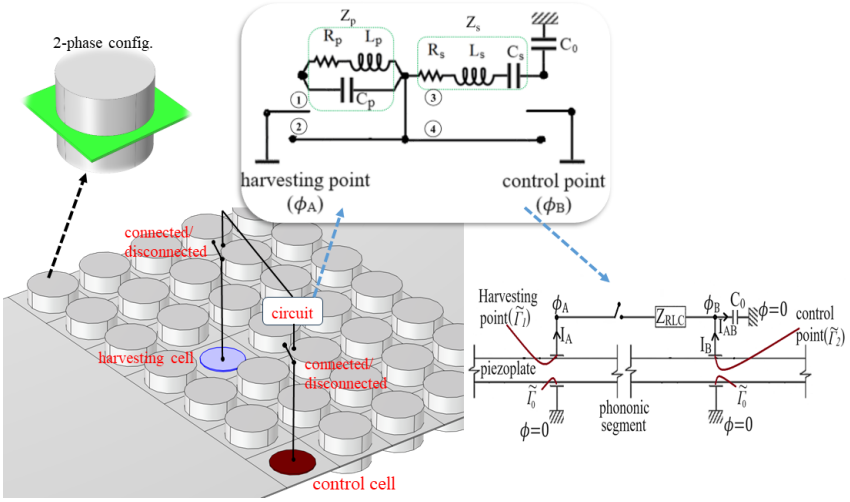

Figure 3: Schematic of the self-powered vibration control and the electrical circuit

electroactive structure to external circuits. These electrodes are considered to be thin enough so their mechanical effects are negligible, and they only act as electrical boundary interfaces. The weak formulation governing the response of the structure has the following form:
find $(\boldsymbol{u}^\varepsilon, \phi^\varepsilon) \in (\boldsymbol{V}_0(\Omega), \Phi_0(\Omega))$ for all $(\boldsymbol{v}, \psi) \in (\boldsymbol{V}_0(\Omega), \Phi_0(\Omega)$ such that:

$$
\begin{aligned}
&-\omega^2 \int_\Omega \rho \boldsymbol{u}\cdot\boldsymbol{v} + \int_\Omega \boldsymbol{\sigma}(\boldsymbol{u},\phi) : \boldsymbol{e}(\boldsymbol{v}) = \int_{\partial\Omega} (\boldsymbol{n}\cdot\boldsymbol{\sigma})\cdot\boldsymbol{v}\,\mathrm{dS} + \int_{\Gamma_\sigma} \boldsymbol{b}\cdot\boldsymbol{v}\,\mathrm{dS}\,,\\
&\int_{\Omega_m} \boldsymbol{D}(\boldsymbol{u},\phi)\cdot\nabla\psi = \sum_{K=A,B} \int_{\Gamma_K} \boldsymbol{D}\cdot\boldsymbol{n}\psi\,\mathrm{dS}\,,
\end{aligned}
\tag{1}
$$

The normal electric displacement $\boldsymbol{D}\cdot\boldsymbol{n}$ at electrode Γ_K is expressed in terms of the electric current I_K, so that

$$
\begin{aligned}
&\mathcal{J}_K(I_K,\psi) := \int_{\Gamma_K} \boldsymbol{D}\cdot\boldsymbol{n}\psi\,\mathrm{dS} = \frac{1}{\mathrm{i}\omega} I_K \bar{\psi}_K\,, \quad K = A, B\,,\\
&I_K = \int_{\Gamma_K} \boldsymbol{j}\cdot\boldsymbol{n}\,\mathrm{dS}\,,
\end{aligned}
\tag{2}
$$

where $\boldsymbol{j}$ denotes the current density. The Kirchhoff's law yields the circuit equations involving currents I_A, I_B and I_C and the two potentials $\overline{\phi}_A$ and $\overline{\phi}_B$,

$$
\begin{aligned}
&I_{A,n} + I_{B,n} = I_{A,n+1}\,,\\
&I_{A,n+1} Z = \varphi_{A,n+1} - \varphi_{A,n}\,,
\end{aligned}
\tag{3}
$$

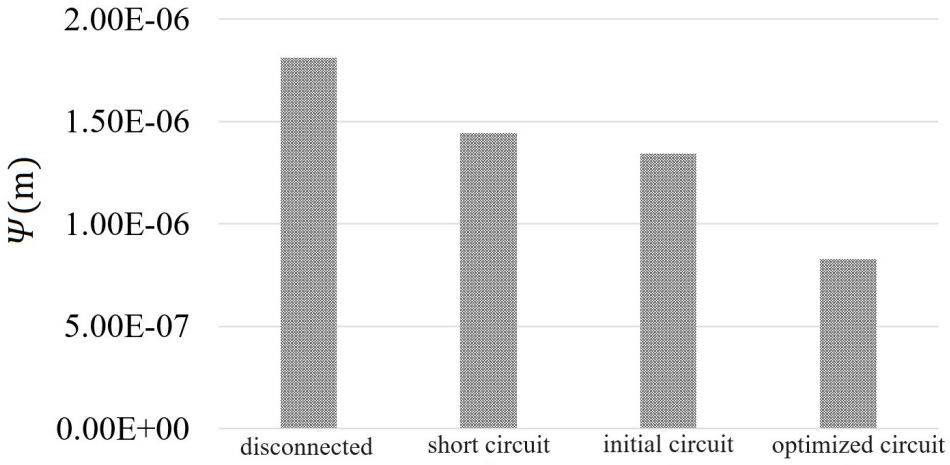

Figure 4: Amplitude of vibration on the control cell for the cases of disconnected, short circuited, connected with initial circuit, and connected with optimized circuit

The dynamic response of the metastructure at the control point is depicted in Fig 4 for several scenarios. For the disconnected circuit, the amplitude of vibrations is 1.80e-6 meters. This amplitude decreases to 1.45e-6 meters and 1.34e-6 meters for the short circuit and initial circuit scenarios, respectively. In the optimized circuit scenario, the amplitude drops from 1.80e-6 meters (disconnected circuit) to 0.83e-6 meters, representing a 54 percentage reduction in vibrations within the control cell.

3 PIEZOELECTRIC METAMATERIAL WITH FLEXOELECTRIC MICROSTRUCTURE

We consider piezoelectric or dielectric materials with a weak flexoelectric property, constituting the skeleton of periodic porous structures which enable to generate the strain gradients. Using the asymptotic homogenization, it is shown that effective behaviour of such materials is piezoelectric, whereby the homogenized piezoelectric coefficients are computed using the characteristic responses of the flexoelectric microstructure.

3.1 Micromodel

The piezo-flexoelectric material model involves the stress σ_{ij} and the electric displacements D_k which are introduced by

$$\begin{aligned} \sigma_{ij} &= C_{ijkl}e_{kl} - \gamma_{ijk}E_k + \mu_{ijkl}\partial_l E_k \ , \\ D_k &= \gamma_{ijk}e_{ij} + \kappa_{kl}E_l + \mu^*_{klij}\partial_l e_{ij} \ , \end{aligned} \tag{4}$$

incorporating the gradients of the strain $e_{ij}(\boldsymbol{u})$ and electric field $E_i(\varphi)$, where

$$\begin{aligned} &E_i(\varphi) = -\partial_i\varphi \ , \text{ electric field } \vec{E} = (E_i) \text{ due to the electric potential } \varphi \ , \\ &e_{ij}(\boldsymbol{u}) = \frac{1}{2}(\partial_j u_i + \partial_i u_j) \ , \text{ strain due to the displacement } \boldsymbol{u} = (u_i) \ . \end{aligned} \tag{5}$$

In general, all the material tensors, *i.e.* $C_{ijkl}, \gamma_{ijk}, \kappa_{kl}$ and $\mu_{ijkl} = \mu^*_{klij}$ are periodically oscillating functions in space, being defined by zero in the voids of the porous material. The displacement $\boldsymbol{u} = (u_i)$ and electric potential φ satisfy the momentum electric charge equilibria

imposed in the solid,

$$\begin{aligned} -\partial_i \sigma_{ij} + \rho \ddot{u}_i &= f_i \ , \\ \partial_k D_k &= q_E \ , \end{aligned} \tag{6}$$

where variables ρ, f_i, and q_E are the density, volume forces and volume electric charge, respectively. The boundary conditions on $\partial_{\text{ext}}\Omega_s \partial = \Omega_s \cap \partial\Omega$, partitioned into non-overlapping subparts Γ_u, Γ_φ and Γ_σ, are given, as follows:

$$\begin{aligned} \boldsymbol{u} &= \boldsymbol{0} \ , \quad \text{on } \Gamma_u \ , \\ \varphi &= \bar{\varphi} \ , \quad \text{on } \Gamma_\varphi \ , \\ n_j \sigma_{ij} &= \hat{b}_i \ , \quad \text{on } \Gamma_\sigma \ , \\ n_i D_i &= \hat{q}_E = 0 \ , \quad \text{on } \Gamma_{E0} \ . \end{aligned} \tag{7}$$

Natural continuity conditions are applied on interfaces Γ_{rs} between different materials (the higher continuity due to the flexoelectric property)

$$\begin{aligned} [n_j \sigma_{ij}] = 0 \ , \quad [n_j D_j] = 0 \ , \\ \left[n_l \mu^*_{klij} e_{ij}\right] = 0 \ , \quad [n_l \mu_{klij} E_i] = 0 \ , \end{aligned} \tag{8}$$

assuming continuous displacement and the el. potential, $[u_i] = 0$, and $[\varphi] = 0$ on any interface Γ_{rs}.

The symmetry in the direct and converse flexoelectric effect yields $\mu^*_{klij} - \mu_{ijkl} = 0$ and the higher order interface conditions

$$\left[n_l \mu^*_{klij} e_{ij}(\boldsymbol{u})\right] = [\mu_{ijkl} \partial_k \varphi n_l] = 0 \ . \tag{9}$$

Under these assumptions, *i.e.* $\mu^*_{klij} = \mu_{ijkl}$ and (9), from (**??**) the uniform estimates with respect to ε (the heterogeneity scale) on the strain $e_{ij}(\boldsymbol{u})$ and electric field $\partial_k \varphi$ can be obtained.

Interfaces of the heterogeneity By the heterogeneity induced interface we mean manifolds $\Gamma_{rs} = \partial\Omega_r \cap \partial\Omega_s$ separating domains Ω_r, Ω_s in which all material parameters are constant, or smoothly varying, while any material parameter can be discontinuous (having a jump) on Γ_{rs}. We assume the following continuity:

$$\begin{aligned} n_k n_l \left[\mu^*_{klij} e_{ij}(\boldsymbol{u})\right] = 0 \ , \\ n_j n_l \left[\mu_{ijkl} \partial_k \varphi\right] = 0 \ . \end{aligned} \tag{10}$$

3.2 Homogenization of periodic porous structures

The solid forms the skeleton of a porous medium which has a periodic structure characterized by length ℓ, such that $\varepsilon = \ell/L$ is small with respect to the "macroscopic" length L. The aim is to obtain a homogenized model representing the porous medium in the limit $\varepsilon \to 0$.

3.2.1 Microstructure

We consider a porous domain $\Omega \subset \mathbb{R}^d$, $d = 2, 3$ occupied by a piezo-flexoelectric solid in $\Omega^\varepsilon_s \subset \Omega$. The material is assumed to be defined by piecewise constant material properties

$C_{ijkl}, \gamma_{ijk}, \kappa_{kl}$ and $\mu_{ijkl} = \mu^*_{klij}$, thus, Ω^ε_s consists of subparts $\Omega^{k,\varepsilon}_s$, labeled by k, with interfaces $\Gamma^\varepsilon_{kl} = \partial\Omega^{k,\varepsilon}_s \cap \partial\Omega^{l,\varepsilon}_s$. The solid skeleton is represented by a periodically heterogeneous continuum generated by copies of the (zoomed) representative periodic cell, $Y =]0, \bar{y}[$, such that $Y_s \subset Y$ is the skeleton and $Y_0 = Y \setminus \overline{Y_s}$ is the void pore. In order to guarantee the strain and electric field gradients are bounded uniformly with respect to ε when $\boldsymbol{\mu} \approx \varepsilon$, we assume the scaling of the unfolded coefficients $\boldsymbol{\mu}^\varepsilon$,

$$\mathcal{T}_\varepsilon\big(\mu^\varepsilon_{ijkl}(x)\big) = \varepsilon\bar{\mu}_{ijkl}(y) \ . \tag{11}$$

The formal homogenization procedure is applied with asymptotic expansions of displacements and electric potential which can be introduced formally,

$$\begin{aligned} \mathcal{T}_\varepsilon(\boldsymbol{u}^\varepsilon) &\approx \boldsymbol{u}^{0\varepsilon}(x) + \varepsilon\boldsymbol{u}^{1\varepsilon}(x,y) + \varepsilon^2\boldsymbol{u}^{2\varepsilon}(x,y) + \dots \ , \\ \mathcal{T}_\varepsilon(\varphi^\varepsilon) &\approx \varphi^{0\varepsilon}(x) + \varepsilon\varphi^{1\varepsilon}(x,y) + \varepsilon^2\varphi^{2\varepsilon}(x,y) + \dots \ , \end{aligned} \tag{12}$$

where $\mathcal{T}_\varepsilon()$ is the unfolding operator, $x \in \Omega$ and $y \in Y_s$. The limit equations can be derived upon substituting (12) into (6). The obtained two-scale model is presented below through the characteristic responses – autonomous solutions (displacements $\boldsymbol{w}, \boldsymbol{z}$, and electric potential ϕ, ζ)of the local microscopic problems, and the macroscopic model governing $(\boldsymbol{u}^0, \varphi^0)$ defined in the homogenized medium Ω. To do so, we employ the following bilinear forms

$$\begin{aligned} a_{Y_s}(\boldsymbol{u}, \boldsymbol{v}) &= \fint_{Y_s} [\mathbb{C}\boldsymbol{e}_y(\boldsymbol{u})] : \boldsymbol{e}_y(\boldsymbol{v}) \,\mathrm{dV}_y \ , \\ g^*_{Y_s}(\boldsymbol{u}, \psi) &= \fint_{Y_s} g^*_{kij} e^y_{ij}(\boldsymbol{u}) \partial^y_k\psi \,\mathrm{dV}_y \ , \\ d_{Y_s}(\varphi, \psi) &= \fint_{Y_s} [\boldsymbol{\kappa}\nabla_y\varphi] \cdot \nabla_y\psi \,\mathrm{dV}_y \ , \\ m_{Y_s}(\psi, \boldsymbol{u}) &= \fint_{Y_s} \bar{\mu}_{ijkl} \partial^y_l\partial^y_k\psi e^y_{ij}(\boldsymbol{u}) \,\mathrm{dV}_y \ , \\ m^*_{Y_s}(\boldsymbol{u}, \psi) &= \fint_{Y_s} \bar{\mu}^*_{klij} \partial^y_l e^y_{ij}(\boldsymbol{u}) \partial^y_k\psi \,\mathrm{dV}_y \ . \end{aligned} \tag{13}$$

Note the symmetry $g_{ijk} = g^*_{kij}$ and $\mu^*_{klij} = \mu_{ijkl}$.

Due to the problem linearity, the two-scale functions can be expressed using the characteristic responses $(\boldsymbol{w}^{ij}, \phi^{ij}) \in \mathbf{H}^1_\#(Y_s) \times H^1_\#(Y_s)$ and $(\boldsymbol{z}^k, \zeta^k) \in \mathbf{H}^1_\#(Y_s) \times H^1_\#(Y_s)$

$$\begin{aligned} \boldsymbol{u}^1 &= \boldsymbol{w}^{ij} e^x_{ij}(\boldsymbol{u}^0) + \boldsymbol{z}^k \partial^x_k\varphi^0 \ , \\ \varphi^1 &= \phi^{ij} e^x_{ij}(\boldsymbol{u}^0) + \zeta^k \partial^x_k\varphi^0 \ , \end{aligned} \tag{14}$$

where the couple $(\boldsymbol{w}^{ij}, \phi^{ij})$ satisfies

$$\begin{aligned} a_{Y_s}\left(\boldsymbol{w}^{ij} + \boldsymbol{\Pi}^{ij}, \boldsymbol{v}\right) + g^*_{Y_s}\left(\boldsymbol{v}, \phi^{ij}\right) - m_{Y_s}\left(\phi^{ij}, \boldsymbol{v}\right) = 0 \ , \quad \forall \boldsymbol{v} \in \mathbf{H}^1_\#(Y_s) \ , \\ g^*_{Y_s}\left(\boldsymbol{w}^{ij} + \boldsymbol{\Pi}^{ij}, \psi\right) - d_{Y_s}\left(\phi^{ij}, \psi\right) + m^*_{Y_s}\left(\boldsymbol{w}^{ij}, \psi\right) = 0 \ , \quad \forall \psi \in H^1_\#(Y_s) \ , \end{aligned} \tag{15}$$

and $(\boldsymbol{z}^k, \zeta^k)$ satisfies

$$\begin{aligned} a_{Y_s}\left(\boldsymbol{z}^k, \boldsymbol{v}\right) + g^*_{Y_s}\left(\boldsymbol{v}, \zeta^k + y_k\right) - m_{Y_s}\left(\zeta^k, \boldsymbol{v}\right) = 0 \ , \quad \forall \boldsymbol{v} \in \mathbf{H}^1_\#(Y_s) \ , \\ g^*_{Y_s}\left(\boldsymbol{z}^k, \psi\right) - d_{Y_s}\left(\zeta^k + y_k, \psi\right) + m^*_{Y_s}\left(\boldsymbol{z}^k, \psi\right) = 0 \ , \quad \forall \psi \in H^1_\#(Y_s) \ . \end{aligned} \tag{16}$$

The effective medium properties are characterized in terms of the homogenized coefficients of a piezoelectric constitutive law involving the elasticity $\mathbb{D}^H = D^H_{ijkl}$, the piezoelectric coupling $\underline{\boldsymbol{G}^H} = (G^H_{ijk})$, $\underline{\boldsymbol{G}^{H*}} = (G^{H*}_{kij})$, and the dielectricity $\boldsymbol{Q}^H = (Q^H_{kl})$. These are expressed through the characteristic solutions of (15) and (16),

$$\begin{aligned} D^H_{klij} &= a_{Y_s}\left(\boldsymbol{w}^{ij} + \boldsymbol{\Pi}^{ij},\, \boldsymbol{\Pi}^{kl}\right) + g^*_{Y_s}\left(\boldsymbol{\Pi}^{kl},\, \phi^{ij}\right) - m_{Y_s}\left(\phi^{ij},\, \boldsymbol{\Pi}^{kl}\right)\ , \\ G^H_{ijk} &= a_{Y_s}\left(\boldsymbol{z}^k,\, \boldsymbol{\Pi}^{ij}\right) + g^*_{Y_s}\left(\boldsymbol{\Pi}^{ij},\, \zeta^k + y_k\right) - m_{Y_s}\left(\zeta^k,\, \boldsymbol{\Pi}^{ij}\right)\ , \\ G^{H*}_{kij} &= g^*_{Y_s}\left(\boldsymbol{w}^{ij} + \boldsymbol{\Pi}^{ij},\, y_k\right) - d_{Y_s}\left(\phi^{ij},\, y_k\right) + m^*_{Y_s}\left(\boldsymbol{w}^{ij},\, y_k\right)\ , \\ -Q^H_{kl} &= g^*_{Y_s}\left(\boldsymbol{z}^k,\, y_l\right) - d_{Y_s}\left(\zeta^k + y_k,\, y_l\right) + m^*_{Y_s}\left(\boldsymbol{z}^k,\, y_l\right)\ . \end{aligned} \tag{17}$$

The macroscopic equations of the homogenized weakly flexoelectric periodic medium attain the following form:

$$\begin{aligned} &\int_\Omega \left(\mathbb{D}^H \boldsymbol{e}(\boldsymbol{u}^0) + \underline{\boldsymbol{G}^H}\nabla\varphi^0\right) : \boldsymbol{e}(\boldsymbol{v}^0) = \int_\Omega (\boldsymbol{f}^H - \rho^H \ddot{\boldsymbol{u}}^0)\ , \\ &\int_\Omega \left(\underline{\boldsymbol{G}^{H*}} : \boldsymbol{e}(\boldsymbol{u}^0) - \boldsymbol{Q}^H\nabla\varphi^0\right)\cdot\nabla\psi^0 = 0\ , \end{aligned} \tag{18}$$

for all $\boldsymbol{v}^0 \in V_0(\Omega)$ and all $\psi^0 \in \Phi_0(\Omega)$.

3.3 1D heterogeneous continuum

We consider rods with periodically varying piece-wise constant cross-section. Equivalently, prismatic rods with periodically varying material properties can be treated by virtue of the 1D reduced model.

3.3.1 Flexoelectric rods with variable cross-sections

Material properties are assumed to be piecewise constant, however, the rod cross-section can vary "arbitrarily" (*e.g.* conic segments); regarding the examples treated in the paper, we consider the decomposition of Y into subsets – segments (rod segments, OR layers) $Y_i =]y_{i-1}, y_i[$, $i = 1, \ldots, n$ with $0 = y_0 < y_1 < \ldots y_n = \bar{y}$, such that $Y = Y_1 \cup \cdots \cup Y_n$ with $Y_i \cap Y_j = \emptyset$ for $i \neq j$, Correspondingly, $\Omega^{k,\varepsilon}_i \subset \Omega$ refers to any real-sized segment, whereby index k refers to the lattice coordinate ξ^k defined above. In this respect, $\Omega \times Y_i$ is the unfolded subdomain involving all i-th layers, thus, representing the union $\bigcup_{k\in\mathbb{Z}} \Omega^{k,\varepsilon}_i$. The modelling is based on the following equations (no piezoelectric effect!)

$$\partial(C_i\partial u - \mu_i\partial^2\varphi) = f\ , \quad \partial(\kappa_i\partial\varphi - \mu_i\partial^2 u) = 0\ , \tag{19}$$

to be satisfied in n sub-intervals $\mathcal{I}_i =]l_i, l_{i+1}[$ of $\hat{\mathcal{I}} = \bigcup_i \mathcal{I}_i$. Potential φ can be eliminated,

$$C_i\partial^2 u - \frac{\mu_i^2}{\kappa_i}\partial^4 u = f\ , \quad \partial^2\varphi = \frac{\mu_i}{\kappa_i}\partial^3 u\ . \tag{20}$$

Obvious integration is applied to derive the week formulation,

$$\begin{aligned} &\sum_i \int_{l_i}^{l_{i+1}} \left(C_i\partial u\partial v + \frac{\mu_i^2}{\kappa_i}\partial^2 u\partial^2 v\right)\mathrm{d}x + \int_{l_0}^{l_n} fv\mathrm{d}x \\ &= \sum_i \left[v\left(C_i\partial u - \frac{\mu_i^2}{\kappa_i}\partial^3 u\right)\right]_{l_i}^{l_{i+1}} - \sum_i \left[\partial v\frac{\mu_i^2}{\kappa_i}\partial^2 u\right]_{l_i}^{l_{i+1}}\ , \end{aligned} \tag{21}$$

for all $v \in H^2(\hat{\mathcal{I}}) \cap H^1(\overline{\mathcal{I}})$ defined piece-wise $H^2(\mathcal{I}_i)$. Hence, the right hand side vanishes if the continuity and periodicity conditions (*i.e.* the cyclic continuity at l_0 matching with l_n) are respected, as follows:

$$\begin{aligned} [u]_\Gamma = 0 \ , \quad [\varphi]_\Gamma = 0 \ , \quad [\partial u]_\Gamma = 0 \ , \quad [\partial \varphi]_\Gamma = 0 \ , \\ [C\partial u - \mu \partial^2 \varphi]_\Gamma = 0 \ , \quad [\kappa \partial \varphi - \mu \partial^2 u]_\Gamma = 0 \ , \end{aligned} \tag{22}$$

where $[\,]_\Gamma$ represents the jump of the argument at any of all interfaces $\Gamma_i = \overline{\mathcal{I}}_{i-1} \cap \overline{\mathcal{I}}_i$ separating the two sub-intervals (note the periodicity at $\Gamma_0 \equiv \Gamma_n$). It is easy to see that the couple (u, φ) is represented by 6 constants at any $\mathcal{I}_i$, so $6n$ constants for the whole rod $]l_0, l_n[$, which are determined due to the $6n$ conditions (22). In the context of the homogenization, analytic solutions of local problems (15)-(16) for such piece-wise homogeneous rods with Y_s represented by $]l_0, l_n[$ can be obtained.

3.3.2 Characteristic responses for the 1D continuum

The homogenization procedure described above leads to the characteristic problems (15) and (16). The characteristic response (w, ϕ) (the strain correctors of the displacement and the electric potential) to the unit macroscopic strain in the 1D continuum is obtained upon solving the following system of equations, incorporating the constitutive laws,

$$\begin{aligned} \sigma_k := C_k(1 + w') - \mu_k \phi'' \ , \quad [\sigma_*] = 0 \ , \\ D_k := \kappa_k \phi' - \mu_k w'' \ , \quad [D_*] = 0 \ , \end{aligned}$$

involved in the equilibrium and charge conservation in all sub-intervals, being supplemented by the interface continuity conditions, as follows,

$$\begin{aligned} (C_k(1 + w') - \mu_k \phi'')' = 0 \ , \quad y \in]y_{k-1}, y_k[\ , \\ (\kappa_k \phi' - \mu_k w'')' = 0 \ , \quad y \in]y_{k-1}, y_k[\ , \\ \text{interfaces: } y^* \in \{y_k\}_{k=0,\dots,n} \ : \quad [w] = [\phi] = 0 \ , \\ [\mu w'] = [\mu \phi'] = 0 \ , \\ [\sigma_*] = 0 \ , \\ [D_*] = 0 \ , \end{aligned}$$

As the matter of fact, for the 1D problem, due to the continuity conditions, the characteristic responses with respect to the macroscopic strain and the electric field are the same. In each sub-interval $]y_{k-1}, y_k[$, the solution is given by

$$\begin{aligned} w_k(y) = \frac{1}{\gamma_k^2} \left(a_k e^{\gamma_k y} + b_k e^{-\gamma_k y} \right) + p_k y + r_k \ , \\ \phi_k(y) = \frac{\mu_k}{\kappa_k} w_k'(y) + q_k y + s_k \ , \end{aligned}$$

where the 6 constants $(a_k, b_k, p_k, r_k, q_k, s_k)$ are determined due to interface conditions and periodicity.

#	D^H	Q^H	G^H
A	1.0	1.0	-3.8276e-06
B	0.81429	0.81429	2.6491e-05

Table 1: Homogenized coefficients: elasticity D^H, dielectricity Q^H, and the piezoelectric coupling G^H for the two microstructures shown in Fig. 5.

3.4 Examples of the homogenized flexoelectric structures

In this section, we aim to illustrate how the effective piezoelectric behaviour observed at the macro-scale depends on the microstructure. We first consider the 1D problem described above. We consider a flexoelectric medium governed by (19)-(22), such that the heterogeneity is generated by piecewise constant, but different cross-section of a periodically heterogeneous rod, as illustrated in Fig. 5. While the the case #A is symmetric (one can define a symmetric cell Y), in the case #B, the structure is non-symmetric. The characteristic solutions for the two cases are illustrated in Fig. 6.

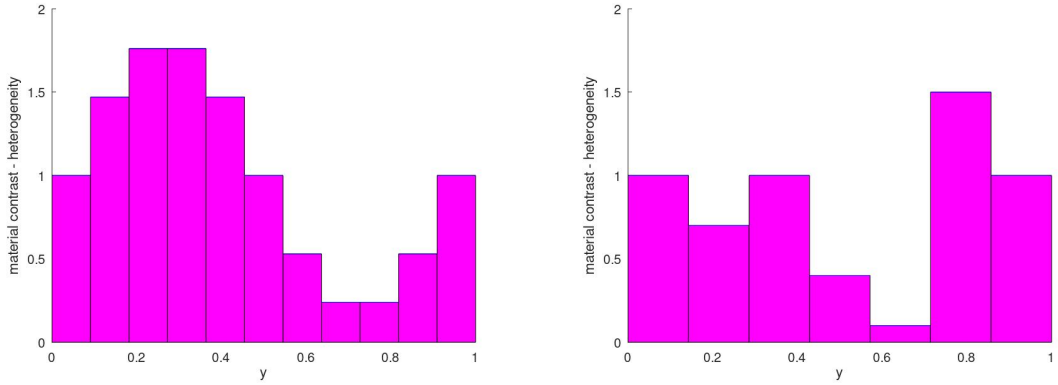

symmetric #A non-symmetric #B

Figure 5: The representative microstructure of the 1D periodic flexoelectric rods.

Tab. 1 shows values of the homogenized coefficients obtained for the two cases for the input values of the microstructure material $C = 1$, $\kappa = 1$ and $\mu = 1$ (measureless) for the scale $\varepsilon_0 = 10^{-3}$:

The 3D case, implemented in the package SfePy [15] using fast tensor contractions [16], is illustrated in Fig. 7 by means of the correctors $(\boldsymbol{z}^k, \zeta^k)$ from (16). Here, the non-symmetric porous structure leads to a non-zero piezo-coupling tensors G^H_{ijk}, G^{H*}_{kij} even for isotropic material parameters on the micro-level.

4 CONCLUSIONS

Electroactive metamaterials (EMM) equipped with an external electric circuit (EEC) show much better efficiency to damp or even stop undesired vibrations in a frequency range. Using optimization of the EEC, band gap frequency ranges can be tuned. As an important feature, so extended optimized EMM operate without any external energy source. The present study proved a great multi-functional potential of the considered self-powered meta-structures for applications requiring simultaneously vibration attenuation and energy harvesting.

Another challenging design option for the EMM design is to use a convenient flexoelectric

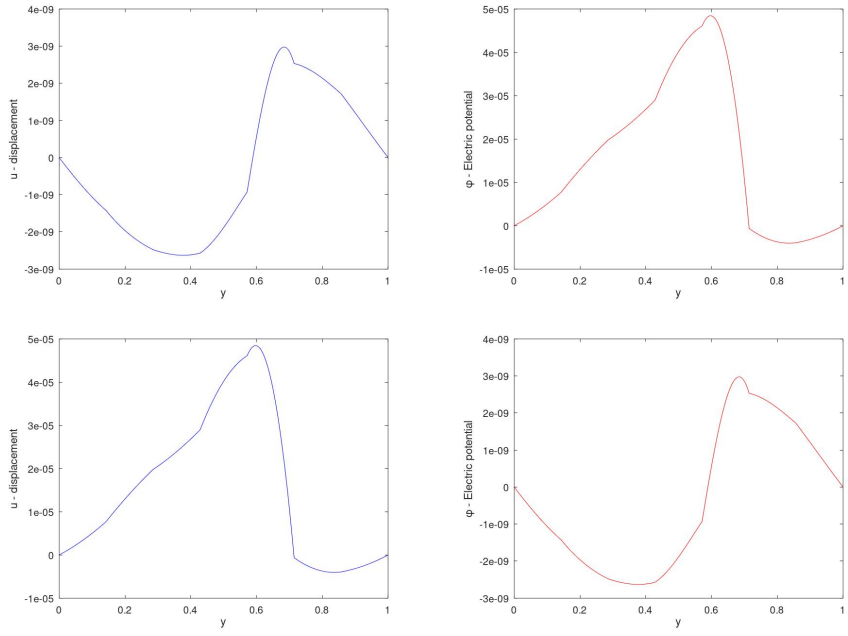

Figure 6: The characteristic responses w and ϕ for the strain and electric field correctors.

material. The homogenized weakly flexoelectric medium provides the piezoelectric (PZ) properties. This can be of interest for various applications based on the PZ sensors or actuators, including devices for the energy harvesting. It has been illustrated that the PZ coupling tensor of the homogenized microstructure depends on the micro-architecture of the porous material – a kind of non-symmetry is required to generate the piezoelectric effect.

Further research will pursue the numerical modelling and optimization of the microstructures to amplify the PZ effect. As pointed out above, for microstructures containing piezoelectric materials, the higher-order homogenization generate the flexoelectric effect (direct and converse). Hence the three scale homogenization via the micro-to-meso and meso-to-macro upscaling using the higher order terms leads to the macroscopic flexoelectric model. The efficiency of so generated flexoelectric effect is to be explored.

Acknowledgement This work has been supported by the grant GACR 23-06220S of the Czech Science Foundation.

REFERENCES

[1] Rohan, E., Miara, B., and Seifrt, F., "Numerical simulation of acoustic band gaps in homogenized elastic composites," *International Journal of Engineering Science*, vol. 47, pp. 573–594, 2009.

[2] Wang, Y.F., Wang, Y.Z.. Wu, B., Chen, W. and Wang, Y.S., "Tunable and active phononic crystals and metamaterials," *Applied Mechanics Reviews*, vol. 72, p. 040801, 02 2020.

[3] Wu, B., Jiang, W., Jiang, J., Zhao, Z., Tang, Y., Zhou, W. and Chen, W., "Wave manipulation in intelligent metamaterials: recent progress and prospects," *Advanced Functional Materials*, vol. 34, no. 29, p. 2316745, 2024.

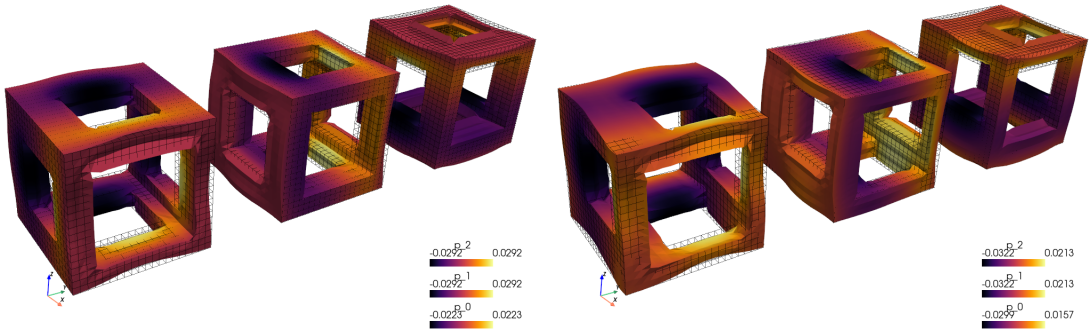

Figure 7: The characteristic responses $(\boldsymbol{z}^k, \zeta^k)$ in a symmetric (left) and non-symmetric (right) 3D porous structure. $\boldsymbol{z}^k$ indicated by mesh deformation, ζ^k by color.

[4] Rohan, E., Cimrman, R., and Miara, B., "Wave propagation and band gaps in homogenized phononic plates—modelling by spectral decomposition," *PAMM*, vol. 14, no. 1, pp. 717–718, 2014.

[5] Hosseinkhani, A. and Rohan, E., "Multi-functional periodically heterogeneous structures for energy harvesting and vibration attenuation-effects of piezoelectricity and shunting circuits," *Smart Materials and Structures*, vol. 33, no. 11, p. 115009, 2024.

[6] Codony, D., Mocci, A., Barceló-Mercader, J., Arias, I., Mathematical and computational modeling of flexoelectricity, Journal of Applied Physics 130 (23) (2021) 231102.

[7] Cioranescu, D., Damlamian, A., Griso, G. (2008), The periodic unfolding method in homogenization. *Siam J. Math. Anal.*, **40**(4):1585–1620.

[8] Rohan, E., Lukeš, V., Homogenization of the fluid-saturated piezoelectric porous media. *International Journal of Solids and Structures*, **147**, 110–125, 2018.

[9] Rohan, E. and Lukeš, V., "Homogenized model of peristaltic deformation driven flows in piezoelectric porous media," *Computers & Structures*, vol. 302, p. 107470, 2024.

[10] Mawassy, N., Reda, H., Ganghoffer, J. F., Eremeyev, V., Lakiss, H., A variational approach of homogenization of piezoelectric composites towards piezoelectric and flexoelectric effective media, International Journal of Engineering Science, 158 (2021) 103410, https://doi.org/10.1016/j.ijengsci.2020.103410.

[11] Guinovart-Sanjuán, D., Merodio, J., López-Realpozo, J.C., Vajravelu, K., Rodríguez-Ramos, R., Guinovart-Díaz, R., Bravo-Castillero, J., Sabina, F.J. Asymptotic Homogenization Applied to Flexoelectric Rods. Materials 2019, 12, 232. https://doi.org/10.3390/ma12020232

[12] Guinovart-Sanjuán, D. Vajravelu, K. et al. Effective predictions of heterogeneous flexoelectric multilayered composite with generalized periodicity. Int J Mech Sci, 181:105755, 2020.

[13] Yvonnet, J., Chen, X. et al. Apparent flexoelectricity due to heterogeneous piezoelectricity. J Appl Mech, 87(11), (2020) 111003.

[14] Mocci, A., Barceló-Mercader, J., Codony, D., Arias, I., Geometrically polarized architected dielectrics with apparent piezoelectricity, Journal of the Mechanics and Physics of Solids 157 (2021) 104643.

[15] Cimrman, R., Lukeš, V., Rohan, E., Multiscale finite element calculations in Python using Sfepy, *Advances in Computational Mathematics*, **45**, 1897–1921, 2019.

[16] Cimrman, R., Fast evaluation of finite element weak forms using python tensor contraction packages, *Advances in Engineering Software*, **159**, 103033, 2021.